

CHALMERS



UNIVERSITY OF GOTHENBURG

PREPRINT 2010:45

A two-model adaptive finite element method for plates

DAVID HEINTZ
PETER HANSBO

*Department of Mathematical Sciences
Division of Mathematics*

CHALMERS UNIVERSITY OF TECHNOLOGY
UNIVERSITY OF GOTHENBURG
Gothenburg Sweden 2010

Preprint 2010:45

**A two-model adaptive finite element method
for plates**

David Heintz, Peter Hansbo

Department of Mathematical Sciences
Division of Mathematics
Chalmers University of Technology and University of Gothenburg
SE-412 96 Gothenburg, Sweden
Gothenburg, December 2010

Preprint 2010:45
ISSN 1652-9715

Matematiska vetenskaper
Göteborg 2010

A two-model adaptive finite element method for plates

David Heintz¹, Peter Hansbo¹

¹ *Department of Mathematics
Chalmers University of Technology and University of Gothenburg
SE-412 96 Göteborg, Sweden*

December 1, 2010

Abstract

We introduce a goal-oriented adaptive finite element method, which combines the Kirchhoff and Mindlin-Reissner plate models. The lateral displacements are approximated by quadratic continuous polynomials, and the rotations of the midsurface are approximated by linear discontinuous polynomials. A duality-based *a posteriori* error representation separates the discretization and modeling errors, and in this sense local mesh and model refinement are independent. The target quantity of interest is an arbitrary linear functional of the displacement and/or rotation errors.

Keywords *Kirchhoff plate, Mindlin-Reissner plate, model adaptivity*

1 Introduction

Two commonly used mathematical models for plate bending problems are the Kirchhoff plate model, applicable to thin plates whose deflections are small, and the Mindlin-Reissner (MR) plate model for thin and moderately thick plates. The Kirchhoff plate model is markedly less expensive to solve numerically, since it only involves the lateral displacements (although it requires C^1 -continuity, which can be computationally cumbersome), whereas the MR plate model also includes the rotations of the midsurface as unknowns. Hence it becomes interesting to adaptively decide which model to use—besides resolving the computational domain—in order to achieve a prescribed accuracy of the discrete solution. Recently it has been suggested in

Heintz [10] to employ the same finite element method for solving a problem in which different models are used in different parts of the physical plate. This idea builds on the continuous/discontinuous Galerkin (c/dG) methods developed by Engel *et al.* [5], and by Hansbo and Larson [8], where continuous \mathcal{P}^d elements (with approximating polynomials of degree d) are used for the lateral displacements. The continuity of the displacement gradient, however, is only weakly imposed in the Kirchhoff plate model [5], corresponding to using discontinuous \mathcal{P}^{d-1} rotations with weakly enforced continuity for the MR plate model [8].

We develop a c/dG finite element method which extends previous work by including goal-oriented adaptivity. The choices of local mesh size and local model are done in an automated way to control arbitrary linear functionals of the displacement and/or rotation errors. The total error is separated into a sum of the discretization and modeling errors, and represents the discrepancy between the discrete solution and the exact solution to a *master model* (which we define to be the MR plate model).

2 The continuous problems

We introduce the continuous problems for the plate models—the strong and the corresponding variational formulations—under the following assumptions: the domain Ω is a convex polygon, clamped at its boundary $\partial\Omega$, i.e., the lateral displacements u and the normal derivative $\partial_n u$ vanish here, and the constitutive parameters λ and μ and the plate thickness t are constants.

The Kirchhoff plate model is described mathematically by a fourth-order partial differential equation,

$$\sum_{ij} \frac{\partial^2 \sigma_{ij}(\nabla u)}{\partial x_i \partial x_j} = f, \quad \text{in } \Omega \subset \mathbb{R}^2, \quad (1)$$

which expresses equilibrium between internal and external forces. Here $t^3 f$ is recognized as the transverse surface load, whereas σ represents the moment tensor,

$$\sigma(\nabla u) := \lambda \nabla \cdot \nabla u \mathbf{1} + 2\mu \varepsilon(\nabla u),$$

for a linearly elastic material. $\mathbf{1}$ is the identity tensor, and ε is the curvature tensor, whose components are

$$\varepsilon_{ij}(\mathbf{v}) := \frac{1}{2} \left(\frac{\partial v_i}{\partial x_j} + \frac{\partial v_j}{\partial x_i} \right), \quad \text{for } i, j = 1, 2.$$

Moreover,

$$\lambda = \frac{E\nu}{12(1-\nu)^2}, \quad \mu = \frac{E}{24(1+\nu)},$$

where E and ν are Young's modulus and Poisson's ratio, respectively. Should shear effects be non-negligible the MR plate model typically replaces (1) to improve the accuracy of the solution. Then we consider instead the system of equations

$$\begin{aligned} -\nabla \cdot \boldsymbol{\sigma}(\boldsymbol{\theta}) - \kappa(\nabla u - \boldsymbol{\theta}) &= \mathbf{0}, \\ -\kappa \nabla \cdot (\nabla u - \boldsymbol{\theta}) &= f, \end{aligned} \tag{2}$$

where $\boldsymbol{\theta}$ denotes the rotations of the midsurface of the plate, and the material parameter

$$\kappa = \frac{Ek}{2t^2(1+\nu)},$$

where $k = 5/6$, is a shear correction factor.

The virtual work equation pertaining to (2) can be derived by minimizing the sum of the bending energy, the potential of the surface load, and the shear energy:

$$(u, \boldsymbol{\theta}) = \min_{v, \boldsymbol{\vartheta}} \mathfrak{F}(v, \boldsymbol{\vartheta}) = \frac{1}{2}a(\boldsymbol{\vartheta}, \boldsymbol{\vartheta}) + \frac{1}{2}b(v, \boldsymbol{\vartheta}; v, \boldsymbol{\vartheta}) - (f, v)_\Omega. \tag{3}$$

v and $\boldsymbol{\vartheta}$ belong to admissible function spaces (to be specified), whereas $(\cdot, \cdot)_\Omega$ represents the L_2 inner product with respect to the indicated domain. The bending energy is defined in terms of the tensor contraction

$$a(\boldsymbol{\theta}, \boldsymbol{\vartheta}) := \int_{\Omega} \boldsymbol{\sigma}(\boldsymbol{\theta}) : \boldsymbol{\varepsilon}(\boldsymbol{\vartheta}) \, d\Omega, \tag{4}$$

and the shear energy is defined by

$$b(u, \boldsymbol{\theta}; v, \boldsymbol{\vartheta}) := \kappa(\nabla u - \boldsymbol{\theta}, \nabla v - \boldsymbol{\vartheta})_\Omega. \tag{5}$$

If (3) is modified by omitting the shear energy functional, and substituting $\boldsymbol{\vartheta} = \nabla v$, we get the corresponding minimization problem for the Kirchhoff plate model,

$$u = \min_v \mathfrak{F}(v) = \frac{1}{2}a(\nabla v, \nabla v) - (f, v)_\Omega. \tag{6}$$

Here the rotation vector is approximated by the displacement gradient, and thus the discrete Kirchhoff solution has less degrees of freedom, but it also requires higher regularity owing to the second-order derivatives present in the bilinear form (4).

Solving (6) and (3) yields the following variational formulations. Firstly, for the Kirchhoff plate model: find $u \in V = \{v \in H_0^2(\Omega) : \partial_n v|_{\partial\Omega} = 0\}$ such that

$$a(\nabla u, \nabla v) = (f, v)_\Omega,$$

for all $v \in V$. Secondly, for the MR plate model, using the function spaces $W = H_0^1(\Omega)$ and $\Theta = W^2$: find $(u, \boldsymbol{\theta}) \in W \times \Theta$ such that

$$a(\boldsymbol{\theta}, \boldsymbol{\vartheta}) + b(u, \boldsymbol{\theta}; v, \boldsymbol{\vartheta}) = (f, v)_\Omega, \quad (7)$$

for all $(v, \boldsymbol{\vartheta}) \in W \times \Theta$.

3 The discrete problems

3.1 The mesh

The computational domain is constructed by partitioning of Ω into a geometrically conforming and quasi-uniform finite element triangulation, $\mathfrak{T}_h = \{T\}$, whose local mesh size is given by

$$h_T := \text{diam}(T) = \max_{\mathbf{y}_1, \mathbf{y}_2 \in T} \|\mathbf{y}_1 - \mathbf{y}_2\|, \quad \text{for all } T \in \mathfrak{T}_h,$$

and let

$$h := \max_{T \in \mathfrak{T}_h} h_T$$

denote the global mesh size parameter. We also define the set of edges in the mesh, $\mathfrak{E} = \{E\}$, which can be divided into two disjoint subsets, $\mathfrak{E} = \mathfrak{E}_I \cup \mathfrak{E}_B$, where $\mathfrak{E}_I = \mathfrak{E} \setminus \partial\Omega$ and \mathfrak{E}_B are the sets of interior edges and boundary edges, respectively. Each edge is associated with a fixed unit normal \mathbf{n} with direction chosen so that \mathbf{n} is the exterior normal on the boundary.

3.2 Function spaces

We introduce the function space

$$V_h := \{v \in \mathcal{C}^0(\Omega) : v|_{\partial\Omega} = 0, v|_T \in \mathcal{P}^d(T) \text{ for all } T \in \mathfrak{T}_h\}$$

of continuous piecewise polynomials of degree d for the approximation of the lateral displacements. For the rotation vector

$$\Theta_h := \{\boldsymbol{\vartheta} \in [L_2(\Omega)]^2 : \boldsymbol{\vartheta}|_T \in [\mathcal{P}^{d-1}(T)]^2 \text{ for all } T \in \mathfrak{T}_h\}$$

is the function space of discontinuous piecewise polynomials of degree $d - 1$. Note how the choice of approximating spaces is compatible in the sense that

$$\nabla v \subset \Theta_h, \quad \text{for all } v \in V_h.$$

This is an important property, since in the limit $t \rightarrow 0$, it allows for functions in Θ_h to belong to ∇V_h . Hence there may exist non-trivial discrete solutions such that the difference $\nabla u - \theta$ in the shear energy functional (5) vanishes, and so shear locking is alleviated.

3.3 Jumps and averages

We introduce two quantities for functions on edges: the jump $[[\cdot]]$ and the average $\langle \cdot \rangle$. For this purpose, let T_1 and T_2 be two neighboring elements, sharing the interior edge E . Now, for a scalar function $v \in V_h$, we define

$$\begin{aligned} [[v]] &:= v^- - v^+, & \text{for } E \in \mathfrak{E}_I, & & [[v]] &:= v^-, & \text{for } E \in \mathfrak{E}_B, \\ \langle v \rangle &:= \frac{1}{2}(v^- + v^+), & \text{for } E \in \mathfrak{E}_I, & & \langle v \rangle &:= v^-, & \text{for } E \in \mathfrak{E}_B, \end{aligned}$$

where

$$v^- = \lim_{\epsilon \rightarrow 0^+} v(\mathbf{x} - \epsilon \mathbf{n}), \quad v^+ = \lim_{\epsilon \rightarrow 0^+} v(\mathbf{x} + \epsilon \mathbf{n}), \quad \text{for } \mathbf{x} = (x, y) \in E.$$

The definitions for a vector-valued function $\boldsymbol{\vartheta} \in \Theta_h$ are analogous.

3.4 The finite element methods

We are ready to formulate the symmetric c/dG finite element methods as follows. Firstly, for the Kirchhoff plate model: find $u^h \in V_h$ such that

$$a_h(\nabla u^h, \nabla v) = (f, v)_\Omega, \tag{8}$$

for all $v \in V_h$. Secondly, for the MR plate model: find $(u^h, \boldsymbol{\theta}^h) \in V_h \times \Theta_h$ such that

$$a_h(\boldsymbol{\theta}^h, \boldsymbol{\vartheta}) + b(u^h, \boldsymbol{\theta}^h; v, \boldsymbol{\vartheta}) = (f, v)_\Omega,$$

for all $(v, \boldsymbol{\vartheta}) \in V_h \times \boldsymbol{\Theta}_h$, where the discrete bilinear form is defined by

$$\begin{aligned}
a_h(\boldsymbol{\theta}^h, \boldsymbol{\vartheta}) &:= \sum_{T \in \mathfrak{T}_h} \int_T \boldsymbol{\sigma}(\boldsymbol{\theta}^h) : \boldsymbol{\varepsilon}(\boldsymbol{\vartheta}) \, dx dy \\
&\quad - \sum_{E \in \mathfrak{E}} (\langle \mathbf{n} \cdot \boldsymbol{\sigma}(\boldsymbol{\theta}^h), [\![\boldsymbol{\vartheta}]\!] \rangle)_E \\
&\quad - \sum_{E \in \mathfrak{E}} (\langle \mathbf{n} \cdot \boldsymbol{\sigma}(\boldsymbol{\vartheta}), [\![\boldsymbol{\theta}^h]\!] \rangle)_E \\
&\quad + (2\mu + 2\lambda)\gamma \sum_{E \in \mathfrak{E}} (h_E^{-1} [\![\boldsymbol{\theta}^h]\!] , [\![\boldsymbol{\vartheta}]\!])_E.
\end{aligned} \tag{9}$$

We remark how the last term in (9) penalizes jumps in the rotation vector (or in the displacement gradient) across element edges, and that the stabilization parameter γ must be chosen large enough to enforce coercivity on the bilinear form, cf. Hansbo and Larson [9]. h_E is given by

$$h_E := \begin{cases} \frac{|T_1| + |T_2|}{2|E|}, & \text{for } E \in \mathfrak{E}_I, \\ |T|/|E|, & \text{for } E \in \mathfrak{E}_B, \end{cases}$$

where $|\cdot|$ denotes either the area of T or the length of E .

Thus far the presentation has treated the Kirchhoff and MR plate models separately. We seek, however, a formulation which combines them, meaning that different elements could be of different types. In order to conveniently characterize such a *simplified model* the model parameter κ^* is introduced, which takes the value

$$\kappa^* := \kappa^*(T) = \begin{cases} \kappa, & \text{if } T \text{ is of MR type,} \\ \alpha\kappa, & \text{if } T \text{ is of Kirchhoff type,} \end{cases}$$

where $\alpha > 0$ is a large number (in the limit $\kappa^* \rightarrow \infty$ the Kirchhoff plate model is regained, owing to the compatibility of the approximating spaces). Hence the simplified model associates the partition \mathfrak{T}_h with a model distribution $\mathfrak{K}_m = \{\kappa^*\}$. The simplified formulation may now be stated as: find $(u^h, \boldsymbol{\theta}^h) \in V_h \times \boldsymbol{\Theta}_h$ such that

$$a_h(\boldsymbol{\theta}^h, \boldsymbol{\vartheta}) + \kappa^*(\nabla u^h - \boldsymbol{\theta}^h, \nabla v - \boldsymbol{\vartheta})_\Omega = (f, v)_\Omega, \tag{10}$$

for all $(v, \boldsymbol{\vartheta}) \in V_h \times \boldsymbol{\Theta}_h$. The difference between (7), the exact solution of the MR plate model, and the discrete solution (10), satisfies the orthogonality relation

$$a_h(e_\theta, \boldsymbol{\vartheta}) + (\kappa(\nabla u - \boldsymbol{\theta}) - \kappa^*(\nabla u^h - \boldsymbol{\theta}^h), \nabla v - \boldsymbol{\vartheta})_\Omega = 0, \tag{11}$$

for all $(v, \boldsymbol{\vartheta}) \in V_h \times \boldsymbol{\Theta}_h$, with the rotation error $\mathbf{e}_\theta = \boldsymbol{\theta} - \boldsymbol{\theta}^h$.

We stress that solving (10) is costly, since *all* elements have an independent approximation of the rotations of the midsurface. In this respect a simplified formulation is better treated as in [10], where Kirchhoff elements only carry degrees of freedom related to lateral displacements. For the practical implementation, we thus introduce a split of \mathfrak{T}_h into one set \mathfrak{T}_h^K containing the Kirchhoff elements, and another set \mathfrak{T}_h^M containing the Mindlin-Reissner elements. The approximation space $\boldsymbol{\Theta}_h$ must then be modified to

$$\boldsymbol{\Theta}_h^M := \{\boldsymbol{\vartheta} \in [L_2(\Omega)]^2 : \boldsymbol{\vartheta}|_T \in [\mathcal{P}^{d-1}(T)]^2 \text{ for all } T \in \mathfrak{T}_h^M\},$$

and the formulation of the discrete problem becomes: find $(u^h, \boldsymbol{\theta}^h) \in V_h \times \boldsymbol{\Theta}_h^M$ such that

$$a_h(\mathcal{F}_T(\boldsymbol{\theta}^h, \nabla u^h), \mathcal{F}_T(\boldsymbol{\vartheta}, \nabla v)) + \sum_{T \in \mathfrak{T}_h^M} \kappa(\nabla u^h - \boldsymbol{\theta}^h, \nabla v - \boldsymbol{\vartheta}) = (f, v)_\Omega, \quad (12)$$

for all $(v, \boldsymbol{\vartheta}) \in V_h \times \boldsymbol{\Theta}_h^M$. Here \mathcal{F}_T is defined elementwise as

$$\mathcal{F}_T(\boldsymbol{\vartheta}, \nabla v) := \begin{cases} \boldsymbol{\vartheta}, & \text{if } T \in \mathfrak{T}_h^M, \\ \nabla v, & \text{if } T \in \mathfrak{T}_h^K. \end{cases}$$

We propose to solve (12) in practice. The more expensive method defined by (10) will be used mainly for the purpose of error analysis (see Section 4.3).

4 *A posteriori* error representations

Following Becker and Rannacher [2], we present two related error representation formulas for control of linear functionals $L_u(e_u)$, where $e_u = u - u^h$, and $L_\theta(\mathbf{e}_\theta)$ of the displacement and rotation errors. In particular, the total error is expressed as a sum of two contributions, identified as the discretization and modeling errors,

$$L(e_u, \mathbf{e}_\theta) := L_u(e_u) + L_\theta(\mathbf{e}_\theta) = e_h + e_m.$$

The error separation provides a means for determining whether an element set for refinement should be divided or, if it is of Kirchhoff type, replaced by a Mindlin element.

4.1 Formula using primal exact and dual simplified solutions

We introduce the dual simplified problem

$$\begin{aligned} -\nabla \cdot \boldsymbol{\sigma}(\boldsymbol{\phi}^*) - \kappa^*(\nabla z^* - \boldsymbol{\phi}^*)_{\Omega} &= J_u, \\ -\kappa^* \nabla \cdot (\nabla z^* - \boldsymbol{\phi}^*)_{\Omega} &= J_{\theta}, \end{aligned}$$

where J_u and J_{θ} are the Riesz representers of L_u and L_{θ} , respectively. The corresponding weak formulation is to find $(z^*, \boldsymbol{\phi}^*) \in W \times \boldsymbol{\Theta}$ such that

$$a(\boldsymbol{\vartheta}, \boldsymbol{\phi}^*) + \kappa^*(\nabla v - \boldsymbol{\vartheta}, \nabla z^* - \boldsymbol{\phi}^*)_{\Omega} = L_u(v) + L_{\theta}(\boldsymbol{\vartheta}), \quad (13)$$

for all $(v, \boldsymbol{\vartheta}) \in W \times \boldsymbol{\Theta}$. Then, since $[\mathbf{n} \cdot \boldsymbol{\phi}^*] = 0$ on the edges, substituting $v = e_u$ and $\boldsymbol{\vartheta} = \mathbf{e}_{\theta}$ in (13) gives

$$\begin{aligned} L(e_u, \mathbf{e}_{\theta}) &= a_h(\mathbf{e}_{\theta}, \boldsymbol{\phi}^*) + \kappa^*(\nabla e_u - \mathbf{e}_{\theta}, \nabla z^* - \boldsymbol{\phi}^*)_{\Omega} \\ &\quad + \kappa(\nabla u - \boldsymbol{\theta}, \nabla z^* - \boldsymbol{\phi}^*)_{\Omega} - \kappa(\nabla u - \boldsymbol{\theta}, \nabla z^* - \boldsymbol{\phi}^*)_{\Omega}, \end{aligned} \quad (14)$$

where the term $\kappa(\nabla u - \boldsymbol{\theta}, \nabla z^* - \boldsymbol{\phi}^*)_{\Omega}$ also has been added and subtracted. Now, let $\pi_z : V \rightarrow V_h$ and $\pi_{\phi} : \boldsymbol{\Theta} \rightarrow \boldsymbol{\Theta}_h$ be standard interpolation operators, use the orthogonality relation (11) with $v = -\pi_z z^*$ and $\boldsymbol{\vartheta} = -\pi_{\phi} \boldsymbol{\phi}^*$, and add

$$0 = a_h(\mathbf{e}_{\theta}, -\pi_{\phi} \boldsymbol{\phi}^*) + (\kappa(\nabla u - \boldsymbol{\theta}) - \kappa^*(\nabla u^h - \boldsymbol{\theta}^h), -(\nabla \pi_z z^* - \pi_{\phi} \boldsymbol{\phi}^*))_{\Omega} \quad (15)$$

to (14). Then

$$\begin{aligned} L(e_u, \mathbf{e}_{\theta}) &= a_h(\mathbf{e}_{\theta}, \boldsymbol{\phi}^* - \pi_{\phi} \boldsymbol{\phi}^*) + \kappa(\nabla u - \boldsymbol{\theta}, \nabla(z^* - \pi_z z^*) - (\boldsymbol{\phi}^* - \pi_{\phi} \boldsymbol{\phi}^*))_{\Omega} \\ &\quad - \kappa^*(\nabla u^h - \boldsymbol{\theta}^h, \nabla(z^* - \pi_z z^*) - (\boldsymbol{\phi}^* - \pi_{\phi} \boldsymbol{\phi}^*))_{\Omega} \\ &\quad + (\kappa^* - \kappa)(\nabla u - \boldsymbol{\theta}, \nabla z^* - \boldsymbol{\phi}^*)_{\Omega}, \end{aligned}$$

where the first two right-hand side terms

$$\begin{aligned} T &= a_h(\mathbf{e}_{\theta}, \boldsymbol{\phi}^* - \pi_{\phi} \boldsymbol{\phi}^*) + \kappa(\nabla u - \boldsymbol{\theta}, \nabla(z^* - \pi_z z^*) - (\boldsymbol{\phi}^* - \pi_{\phi} \boldsymbol{\phi}^*))_{\Omega} \\ &= (f, z^* - \pi_z z^*)_{\Omega} - a_h(\boldsymbol{\theta}^h, \boldsymbol{\phi}^* - \pi_{\phi} \boldsymbol{\phi}^*), \end{aligned} \quad (16)$$

by (7), i.e.,

$$\begin{aligned} L(e_u, \mathbf{e}_{\theta}) &= (f, z^* - \pi_z z^*)_{\Omega} - a_h(\boldsymbol{\theta}^h, \boldsymbol{\phi}^* - \pi_{\phi} \boldsymbol{\phi}^*) \\ &\quad - \kappa^*(\nabla u^h - \boldsymbol{\theta}^h, \nabla(z^* - \pi_z z^*) - (\boldsymbol{\phi}^* - \pi_{\phi} \boldsymbol{\phi}^*))_{\Omega} \\ &\quad + (\kappa^* - \kappa)(\nabla u - \boldsymbol{\theta}, \nabla z^* - \boldsymbol{\phi}^*)_{\Omega}. \end{aligned} \quad (17)$$

In (17) we can identify two error contributions. Firstly, how well the computed solution of the simplified formulation satisfies the exact solution of the simplified formulation, i.e., the discretization error

$$e_h = (f, z^* - \pi_z z^*)_\Omega - a_h(\boldsymbol{\theta}^h, \boldsymbol{\phi}^* - \pi_\phi \boldsymbol{\phi}^*) - \kappa^* (\nabla u^h - \boldsymbol{\theta}^h, \nabla(z^* - \pi_z z^*) - (\boldsymbol{\phi}^* - \pi_\phi \boldsymbol{\phi}^*))_\Omega.$$

Secondly, we have

$$e_m = (\kappa^* - \kappa)(\nabla u - \boldsymbol{\theta}, \nabla z^* - \boldsymbol{\phi}^*)_\Omega,$$

which corresponds to the modeling error, measuring how well the simplified model approximates the exact model. By introducing the primal exact and dual simplified shear forces,

$$\boldsymbol{\zeta}_u := \kappa(\nabla u - \boldsymbol{\theta}) \quad \text{and} \quad \boldsymbol{\zeta}_{z^*} := \kappa^*(\nabla z^* - \boldsymbol{\phi}^*),$$

respectively, we can rewrite

$$e_m = (\boldsymbol{\zeta}_{z^*}, \nabla u - \boldsymbol{\theta})_\Omega - (\boldsymbol{\zeta}_u, \nabla z^* - \boldsymbol{\phi}^*)_\Omega. \quad (18)$$

Thus the modeling error, with respect to $L(e_u, \mathbf{e}_\theta)$, is measured by the difference between the work done by the dual simplified shear force on the primal exact shear angle $\nabla u - \boldsymbol{\theta}$, and the work done by the primal exact shear force on the dual simplified shear angle $\nabla z^* - \boldsymbol{\phi}^*$.

4.2 Formula using dual exact solution

Alternatively an error representation can be derived by using a dual Mindlin-Reissner problem. To this end, consider the problem

$$\begin{aligned} -\nabla \cdot \boldsymbol{\sigma}(\boldsymbol{\phi}) - \kappa(\nabla z - \boldsymbol{\phi})_\Omega &= J_u, \\ -\kappa \nabla \cdot (\nabla z - \boldsymbol{\phi})_\Omega &= J_\theta, \end{aligned}$$

the weak formulation of which is to find $(z, \boldsymbol{\phi}) \in W \times \boldsymbol{\Theta}$ such that

$$a(\boldsymbol{\vartheta}, \boldsymbol{\phi}) + \kappa(\nabla v - \boldsymbol{\vartheta}, \nabla z - \boldsymbol{\phi})_\Omega = L_u(v) + L_\theta(\boldsymbol{\vartheta}), \quad (19)$$

for all $(v, \boldsymbol{\vartheta}) \in W \times \boldsymbol{\Theta}$. Using the displacement and rotation errors as test functions in (19) leads to

$$\begin{aligned} L(e_u, \mathbf{e}_\theta) &= a_h(\mathbf{e}_\theta, \boldsymbol{\phi}) + \kappa(\nabla e_u - \mathbf{e}_\theta, \nabla z - \boldsymbol{\phi})_\Omega \\ &\quad + \kappa^*(\nabla u^h - \boldsymbol{\theta}^h, \nabla z - \boldsymbol{\phi})_\Omega - \kappa^*(\nabla u^h - \boldsymbol{\theta}^h, \nabla z - \boldsymbol{\phi})_\Omega, \end{aligned} \quad (20)$$

by adding and subtracting the term $\kappa^*(\nabla u^h - \boldsymbol{\theta}^h, \nabla z - \boldsymbol{\phi})_\Omega$. Next add the zero-contribution (15)—with $(z, \boldsymbol{\phi})$ replacing $(z^*, \boldsymbol{\phi}^*)$ (here and in the sequel where appropriate)—to (20), which yields

$$\begin{aligned} L(e_u, \mathbf{e}_\theta) &= a_h(\mathbf{e}_\theta, \boldsymbol{\phi} - \pi_\phi \boldsymbol{\phi}) + \kappa(\nabla u - \boldsymbol{\theta}, \nabla(z - \pi_z z) - (\boldsymbol{\phi} - \pi_\phi \boldsymbol{\phi}))_\Omega \\ &\quad - \kappa^*(\nabla u^h - \boldsymbol{\theta}^h, \nabla(z - \pi_z z) - (\boldsymbol{\phi} - \pi_\phi \boldsymbol{\phi}))_\Omega \\ &\quad + (\kappa^* - \kappa)(\nabla u^h - \boldsymbol{\theta}^h, \nabla z - \boldsymbol{\phi})_\Omega, \end{aligned}$$

and by (16)

$$\begin{aligned} L(e_u, \mathbf{e}_\theta) &= (f, z - \pi_z z)_\Omega - a_h(\boldsymbol{\theta}^h, \boldsymbol{\phi} - \pi_\phi \boldsymbol{\phi}) \\ &\quad - \kappa^*(\nabla u^h - \boldsymbol{\theta}^h, \nabla(z - \pi_z z) - (\boldsymbol{\phi} - \pi_\phi \boldsymbol{\phi}))_\Omega \quad (21) \\ &\quad + (\kappa^* - \kappa)(\nabla u^h - \boldsymbol{\theta}^h, \nabla z - \boldsymbol{\phi})_\Omega. \end{aligned}$$

In (21) we readily identify the discretization error

$$\begin{aligned} e_h &= (f, z - \pi_z z)_\Omega - a_h(\boldsymbol{\theta}^h, \boldsymbol{\phi} - \pi_\phi \boldsymbol{\phi}) \\ &\quad - \kappa^*(\nabla u^h - \boldsymbol{\theta}^h, \nabla(z - \pi_z z) - (\boldsymbol{\phi} - \pi_\phi \boldsymbol{\phi}))_\Omega, \end{aligned}$$

and as for the modeling error,

$$e_m = (\kappa^* - \kappa)(\nabla u^h - \boldsymbol{\theta}^h, \nabla z - \boldsymbol{\phi})_\Omega.$$

Defining the primal simplified and dual exact shear forces,

$$\boldsymbol{\zeta}_{u^h} := \kappa^*(\nabla u^h - \boldsymbol{\theta}^h) \text{ and } \boldsymbol{\zeta}_z := \kappa(\nabla z - \boldsymbol{\phi}),$$

respectively, allows us to rewrite

$$e_m = (\boldsymbol{\zeta}_{u^h}, \nabla z - \boldsymbol{\phi})_\Omega - (\boldsymbol{\zeta}_z, \nabla u^h - \boldsymbol{\theta}^h)_\Omega, \quad (22)$$

i.e., the modeling error with respect to $L(e_u, \mathbf{e}_\theta)$ is measured by the difference between the work done by the primal simplified shear force on the dual exact shear angle $\nabla z - \boldsymbol{\phi}$, and the work done by the dual exact shear force on the primal simplified shear angle $\nabla u^h - \boldsymbol{\theta}^h$ (whereas (18) involves the primal exact shear angle).

4.3 Remarks

The exact solutions in (17) and (21) are all *a priori*, and thus in general need to be approximated by enhanced discrete solutions, followed by element- and edgewise evaluation to estimate the error and obtain local error indicators.

Note that the evaluation of (17), besides the primal simplified solution, requires *both* the primal exact and the dual simplified solutions, whereas the evaluation of (21) only requires the dual exact solution. Hence an adaptive method based on (21) would appear to be the less expensive strategy. There is, however, a practical difficulty, namely how to compute the simplified shear forces: Kirchhoff elements approximated using the finite element method (8) lose the modeling error information (since then $\zeta_{z^*} = 0$ in (18) or $\zeta_{u^h} = 0$ in (22)). We address the problem by solving the simplified formulation (10) for the enhanced discrete solutions (u_a, θ_a) and (z_a^*, ϕ_a^*) . Then *every* element carries degrees of freedom related to the rotations of the midsurface, which is expensive, but more importantly it retrieves the non-zero simplified shear forces on Kirchhoff elements. To reduce the computational cost, though, we propose to solve local Dirichlet problems on refined element patches for the enhanced discrete solutions, being a standard approach to error estimation, cf. Verfürth [13].

We opt for (17) in favor of (21), since our strategy would require computing the shear forces ζ_{u^h} by solving (10) *globally* (without Kirchhoff elements) to obtain (u^h, θ^h) , which is not feasible.

5 Implementation

We establish an adaptive method based on (17), which requires approximations of the unknown primal exact and dual simplified solutions.

Firstly, the primal *and* dual simplified formulations (12) are solved—with different load vectors—using the same initial mesh and model distribution $(\mathfrak{T}_h^i, \mathfrak{K}_m^i)$. The Cholesky factorizations of the stiffness matrices will be the same, and thus the additional cost of solving for (z^h, ϕ^h) is negligible. The solutions (u^h, θ^h) and (z^h, ϕ^h) are used for applying fixed boundary conditions in the local Dirichlet problems. Next each element (parent) $T_j \in \mathfrak{T}_h^i$, $j = 1, 2, \dots, N_{\text{ele}}$, is split by regular refinement into four elements (children), and then element patches \mathfrak{P}^j are constructed. These patches must not be too small—if so the enhanced simplified solutions get to few additional degrees of freedom, and the local error indicators become less accurate. In general it does not suffice for patches to consist of a single parent element, as shown in Figure 1. Here it is due to the jump in the linear rotation components, between the children and their parent, being penalized along the boundary. Consequently, for large stabilization parameters, $(\theta_a, \phi_a^*) \rightarrow (\theta^h, \phi^h)$, i.e., *all* degrees of freedom are (weakly) prescribed. To circumvent this problem we also include every parent that connects to any vertex of T_j in the patch,

as exemplified in Figure 2. On each patch (10) is solved for enhanced primal exact and dual simplified solutions, whose restrictions to T_j , $(u_a, \boldsymbol{\theta}_a)|_{T_j}$ and $(z_a^*, \boldsymbol{\phi}_a^*)|_{T_j}$, will be used to estimate the total error (leading to globally discontinuous lateral displacements). We emphasize that solving local Dirichlet problems is suitable for parallelization.

When evaluating the error representation (17), we let $\pi_z z^*$ and $\pi_\phi \boldsymbol{\phi}^*$ be the nodal interpolation of z_a^* and the L_2 projection of $\boldsymbol{\phi}_a^*$, respectively. The discretization errors emanating from internal edges are split between neighbors. Each element T_j contributes $\eta_j = \eta_{j,h} + \eta_{j,m}$ to the total error,

$$L(e_u, \mathbf{e}_\theta) \approx \sum_{j=1}^{N_{\text{ele}}} \eta_j = L(u_a - u^h, \boldsymbol{\theta}_a - \boldsymbol{\theta}^h),$$

and the stopping criterion of the adaptive algorithm, summarized in Algorithm 1, is imposed on the relative total error,

$$\text{TOL} \leq e_{\text{rel}} := \left| \frac{L(u_a - u^h, \boldsymbol{\theta}_a - \boldsymbol{\theta}^h)}{L(u_a, \boldsymbol{\theta}_a)} \right|, \quad (23)$$

where TOL is a prescribed tolerance. Should (23) not be satisfied at the i :th refinement level, the elements corresponding to a (approximatively) fixed-ratio $r = 20\%$ of the largest absolute local error indicators,

$$\{|\eta_{1,h}|, \dots, |\eta_{N_{\text{ele}},h}|, |\eta_{1,m}|, \dots, |\eta_{N_{\text{ele}},m}|\},$$

are locally refined by longest-edge bisection and/or model refinement.

To measure the accuracy of the resulting local error indicators we use an effectivity index,

$$I_{\text{eff}} := \frac{L(u_a - u^h, \boldsymbol{\theta}_a - \boldsymbol{\theta}^h)}{L(e_u, \mathbf{e}_\theta)},$$

which desirably is close to unity (depending on how well $(u_a, \boldsymbol{\theta}_a)$ and $(z_a^*, \boldsymbol{\phi}_a^*)$ approximate the *a priori* terms). Should an analytical solution not be available, the exact error in the target quantity is approximated using a computed solution, $L(\tilde{u}, \tilde{\boldsymbol{\theta}})$, with respect to a densely adapted mesh and model distribution. Then $L(e_u, \mathbf{e}_\theta) \approx L(\tilde{u} - u^h, \tilde{\boldsymbol{\theta}} - \boldsymbol{\theta}^h)$ and $I_{\text{eff}} \approx \tilde{I}_{\text{eff}}$.

For more sophisticated refinement strategies, which, e.g., include coarsening and try to balance the total error, we refer to Bangerth and Rannacher [1] for an overview. In particular, we would consider coarsening of the model (so that in each refinement level, $r \geq X \geq Y \geq 0$, where X and Y are the fractions of Kirchhoff and Mindlin elements set to be refined and coarsened, respectively), due to the limited size of the model hierarchy.

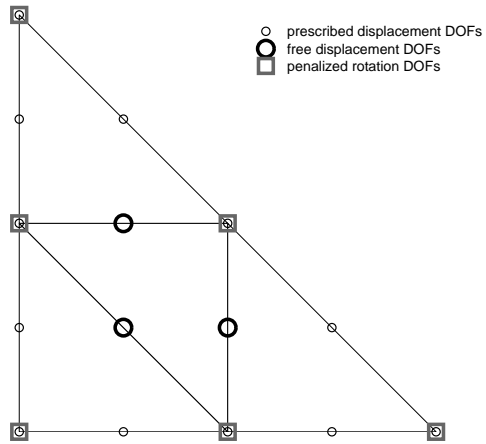


Figure 1: *Solving local Dirichlet problems on single parent elements means that all rotation degrees of freedom (DOFs) will be (weakly) prescribed.*

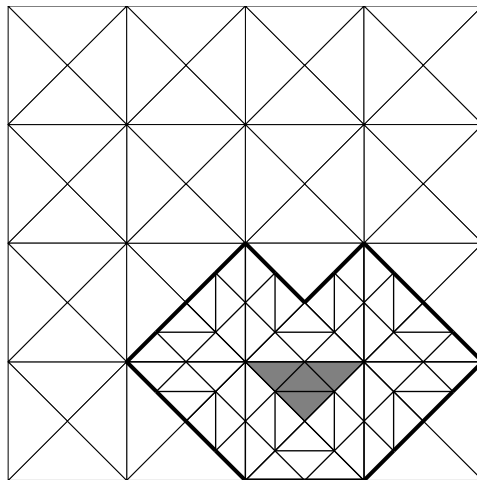


Figure 2: *Element patch consisting of every parent connecting to any vertex of the grey marked parent.*

Algorithm 1: *Adaptive scheme*

Data: $(\mathfrak{T}_h^0, \mathfrak{R}_m^0)$, TOL
Result: $(u^h, \boldsymbol{\theta}^h)$, $L(u^h, \boldsymbol{\theta}^h)$, $L(u_a - u^h, \boldsymbol{\theta}_a - \boldsymbol{\theta}^h)$

for $i = 0, 1, \dots$ **do**
 solve (12) for $(u^h, \boldsymbol{\theta}^h)$ and $(z^h, \boldsymbol{\phi}^h)$ on $(\mathfrak{T}_h^i, \mathfrak{R}_m^i)$;
 construct element patches \mathfrak{P}^j ;
 forall the element patches do
 | solve (10) for $(u_a, \boldsymbol{\theta}_a)|_{T_j}$ and $(z_a^*, \boldsymbol{\phi}_a^*)|_{T_j}$ on \mathfrak{P}^j ;
 end
 compute $\{\eta_{j,h}\}$, $\{\eta_{j,m}\}$ and e_{rel} by evaluating (17);
 if stopping criterion (23) is not satisfied then
 | refine mesh and/or model locally: $(\mathfrak{T}_h^i, \mathfrak{R}_m^i) \rightarrow (\mathfrak{T}_h^{i+1}, \mathfrak{R}_m^{i+1})$;
 else
 | break (target quantity is within the prescribed tolerance);
 end
end

6 Numerical examples

Algorithm 1 is applied to two prototypical model problems to exemplify the behavior of the adaptive procedure.

In all problems the material parameters $E = 1$, $\nu = 1/3$ and $k = 5/6$, the stability parameter $\gamma = 10(2\lambda + 2\mu)d^2$, the model parameter $\alpha = 10^6$, and the plate thickness $t = 10^{-2}$.

The plate will be clamped, and thus large shear forces can be expected along the boundary of the domain. The initial model distribution therefore comprises a boundary layer of Mindlin elements, as shown in Figures 5 and 10.

The target quantity is chosen to be a linear functional of the lateral displacements, i.e., $J_\theta = \mathbf{0}$.

6.1 An L-shaped membrane

The polygonal domain Ω has vertices at

$$(0, 0), (1/2, 0), (1/2, 1/2), (1, 1/2), (1, 1) \text{ and } (0, 1).$$

The plate is subjected to the uniform transverse load $f = 1$, likewise for the dual problem with right-hand side $J_u = 1$, which means

$$L(e_u, \mathbf{e}_\theta) = \int_{\Omega} (u - u^h) \, d\Omega,$$

so we are controlling the error in the mean lateral displacement. A computed solution to this problem can be found in Hansbo *et al.* [7].

The initial and the adapted meshes at the fifth refinement level are shown in Figures 3 and 4, respectively. Local refinement is prominent at the interior corner, in the presence of a stress singularity, and along the boundary of the domain. The initial model and the distribution at the fifth refinement level are shown in Figures 5 and 6. In beginning of the adaptive procedure the total error is underestimated, but the effectivity index stabilizes at $\tilde{I}_{\text{eff}} \approx 1.1$, as tabulated in Table 1.

We try to estimate how solving local Dirichlet problems affects performance in terms of execution time. This is done in a straightforward way by measuring the time it takes to solve the linear system, or systems, of equations for an enhanced primal exact solution $(u_a, \boldsymbol{\theta}_a)$.

The total execution times, either by solving the systems on each element patch, or by solving the global system, are listed and compared in Table 2. The benchmark indicates that solving local Dirichlet problems *in parallel* becomes faster as the size of the global problem increases (the execution time grows linearly with the number of patches). On the test system with 4 Intel Xeon X5650@2.67GHz CPUs, 48 GB RAM, running RHEL 5.5, solving local Dirichlet problems on 8 cores would be faster starting at the fifth refinement level, assuming perfect scaling.

We stress that the time required to construct element patches, and the time needed to perform the assembly processes, are not taken into account (the solution step, however, is the most expensive). Neither is the approximation of the enhanced dual simplified solution (z_a^*, ϕ_a^*) . (Notice that the sparsity patterns of the dual stiffness matrices are the same as their primal counterparts, and thus the same reordering can be applied before factorization to reduce fill-in.)

We have used CHOLMOD, see Chen *et al.* [3], for factorizing the sparse symmetric positive definite matrices (a direct solver which is not parallel). For larger problems, especially in 3D, solving the global system using sparse iterative solvers could be beneficial.

6.2 The unit square

Let $\Omega = [0, 1] \times [0, 1]$. The plate is subjected to the transverse surface load

$$f = \frac{E}{12(1-\nu^2)} \left(12y(y-1)(5x^2-5x+1) \times \right. \\ \left. (2y^2(y-1)^2 + x(x-1)(5y^2-5y+1)) + \right. \\ \left. 12x(x-1)(5y^2-5y+1) \times \right. \\ \left. (2x^2(x-1)^2 + y(y-1)(5x^2-5x+1)) \right).$$

The primal exact solutions were stated by Chinosi *et. al.* [4]: For the lateral displacements,

$$u(x, y) = u_0(x, y) + u_r(x, y),$$

where the first term corresponds to the Kirchhoff solution,

$$u_0(x, y) = \frac{1}{3}x^3(x-1)^3y^3(y-1)^3,$$

and the remainder term

$$u_r(x, y) = -\frac{2t^2}{5(1-\nu)} \left(y^3(y-1)^3x(x-1)(5x^2-5x+1) + \right. \\ \left. x^3(x-1)^3y(y-1)(5y^2-5y+1) \right);$$

and for the rotations of the midsurface

$$\boldsymbol{\theta}(x, y) = \begin{bmatrix} y^3(y-1)^3x^2(x-1)^2(2x-1) \\ x^3(x-1)^3y^2(y-1)^2(2y-1) \end{bmatrix}.$$

The datum of the dual plate problem is chosen to be a Dirac delta function, $J_u = \delta(x - \bar{x}, y - \bar{y})$, where (\bar{x}, \bar{y}) is the point of maximum lateral displacement, and the target quantity simplifies to $L(e_u, e_\theta) = u(\bar{x}, \bar{y}) - u^h(\bar{x}, \bar{y})$.

The model problem is solved adaptively by approximating the *a priori* terms, for the sake of comparison, both on element patches and globally. The final meshes, which are shown in Figures 8 and 9, are densely refined around (\bar{x}, \bar{y}) . In the final model distributions, seen in Figures 11 and 12, Mindlin elements have been introduced in regions with large transverse forces, in accordance with [10]. The effectivity indices, listed in Tables 3 and 4, are close to unity—when evaluating (17) using enhanced discrete solutions obtained by solving local Dirichlet problems, however, the total error is estimated to be slightly smaller.

7 Conclusions

The proposed adaptive finite element method shows promise, as the evaluation of the underlying *a posteriori* error representation can produce accurate local error indicators. The strategy requires the solution of a costly simplified plate formulation to recover the simplified shear forces, however, but the performance in terms of speed can be enhanced by, e.g., solving parallelized local Dirichlet problems. Thereby the proposed method becomes more of an option for practical computations.

References

- [1] *Bangerth B, Rannacher R.* Adaptive finite element methods for differential equations. *Birkhäuser Verlag, Basel.* 2003.
- [2] *Becker R, Rannacher R.* A feed-back approach to error control in finite element methods: basic analysis and examples. *East-West J. Numer. Math.* 1996; **4**:237-264.
- [3] *Chen Y, Davis T, Hager W, Rajamanickam S.* Algorithm 887: CHOLMOD, supernodal sparse Cholesky factorization and update/downdate. *ACM Trans. Math. Software*, Vol. 35, No. 3, 2009.
- [4] *Chinosi C, Lovadina C, Marini LD.* Nonconforming locking-free finite elements for Reissner-Mindlin plates. *Comput. Methods Appl. Mech. Engrg.* 2006; **195**:3448-3460.
- [5] *Engel G, Garikipati K, Hughes TJR, Larson MG, Mazzei L, Taylor RL.* Continuous/discontinuous finite element approximations of fourth-order elliptic problems in structural and continuum mechanics with applications to thin beams and plates, and strain gradient elasticity. *Comput. Methods Appl. Mech. Engrg.* 2002; **191**:3669-3750.
- [6] *Hansbo P, Heintz D, Larson MG.* An adaptive finite element method for second order plate theory. *Internat. J. Numer. Methods Engrg.* 2010; **81**:584-603.
- [7] *Hansbo P, Heintz D, Larson MG.* A finite element method with discontinuous rotations for the Mindlin-Reissner plate model. *Comput. Methods Appl. Mech. Engrg.* To appear; doi:10.1016/j.cma.2010.09.009.

- [8] *Hansbo P, Larson MG.* A \mathcal{P}^2 -continuous, \mathcal{P}^1 -discontinuous Galerkin method for the Mindlin-Reissner plate model. *Brezzi F, Buffa A, Corsaro S, Murli A (eds): Numerical Mathematics and Advanced Applications, Springer, Milan.* 2003; 765-774.
- [9] *Hansbo P, Larson MG.* A discontinuous Galerkin method for the plate problem. *Calcolo.* 2002; **39**:41-59.
- [10] *Heintz D.* Model adaptivity for plates based on a continuous-discontinuous finite element method. *Preprint 2010:33, Department of Mathematical Sciences, Chalmers University of Technology and University of Gothenburg.*
- [11] *Larson MG, Bengzon F.* Adaptive finite element approximation of multiphysics problems. *Comm. Numer. Methods Engrg.* 2008; **24**:505-521.
- [12] *Nitsche, J.* Über ein Variationsprincip zur Lösung von Dirichlet-Problemen bei Verwendung von Teilräumen, die keinen Randbedingungen unterworfen sind. *Abh. Math. Sem. Univ. Hamburg.* 1971; **36**:9-15.
- [13] *Verfürth R.* A review of a posteriori error estimation and adaptive mesh-refinement techniques. *Wiley-Teubner.* 1996.
- [14] *Zhang S.* On the accuracy of Reissner-Mindlin plate model for stress boundary conditions. *ESAIM: Mathematical Modelling and Numerical Analysis.* 2006; **40**:269-294.

Table 1: Data during adaptive procedure when solving the model problem in Section 6.1. The error representation (17) was evaluated using enhanced discrete solutions, which were obtained by solving local Dirichlet problems. (i is the refinement level; N_{ele} is the number of elements; L is the target quantity, the mean lateral displacement; e_{rel} is its relative error; and \tilde{I}_{eff} is the effectivity index.)

i	N_{ele}	# nodes	# DOFs	$L(u^h, \theta^h)$	e_{rel}	\tilde{I}_{eff}
1	768	1 601	1 985	$5.38 \cdot 10^{-4}$	$3.13 \cdot 10^{-2}$	0.29
2	866	1 827	3 003	$5.62 \cdot 10^{-4}$	$3.95 \cdot 10^{-2}$	0.57
3	1 080	2 265	4 401	$5.73 \cdot 10^{-4}$	$3.13 \cdot 10^{-2}$	0.61
4	1 376	2 873	6 161	$5.81 \cdot 10^{-4}$	$2.50 \cdot 10^{-2}$	0.64
5	1 768	3 689	8 789	$5.86 \cdot 10^{-4}$	$2.11 \cdot 10^{-2}$	0.68
6	2 256	4 703	12 179	$5.89 \cdot 10^{-4}$	$1.74 \cdot 10^{-2}$	0.70
7	2 818	5 853	16 125	$5.93 \cdot 10^{-4}$	$1.47 \cdot 10^{-2}$	0.75
8	3 554	7 347	21 603	$5.95 \cdot 10^{-4}$	$1.28 \cdot 10^{-2}$	0.80
9	4 576	9 431	29 003	$5.97 \cdot 10^{-4}$	$1.04 \cdot 10^{-2}$	0.87
10	5 920	12 185	39 245	$5.99 \cdot 10^{-4}$	$7.97 \cdot 10^{-3}$	0.92
11	7 628	15 659	52 295	$6.01 \cdot 10^{-4}$	$6.07 \cdot 10^{-3}$	0.96
12	9 672	19 787	68 633	$6.02 \cdot 10^{-4}$	$4.61 \cdot 10^{-3}$	0.98
13	12 616	25 713	91 875	$6.02 \cdot 10^{-4}$	$3.59 \cdot 10^{-3}$	1.04
14	16 758	34 129	124 867	$6.03 \cdot 10^{-4}$	$2.68 \cdot 10^{-3}$	1.08
15	22 314	45 387	168 333	$6.03 \cdot 10^{-4}$	$1.95 \cdot 10^{-3}$	1.11
16	29 176	59 215	221 785	$6.04 \cdot 10^{-4}$	$1.36 \cdot 10^{-3}$	1.09
17	39 132	79 173	299 511	$6.04 \cdot 10^{-4}$	$9.96 \cdot 10^{-4}$	1.08

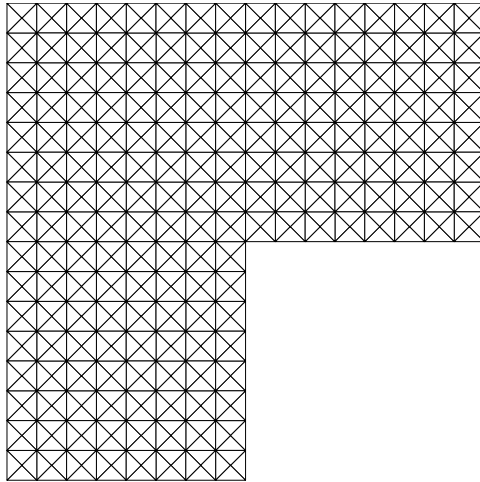


Figure 3: *The initial mesh \mathfrak{T}_h^0 when solving the model problem in Section 6.1.*

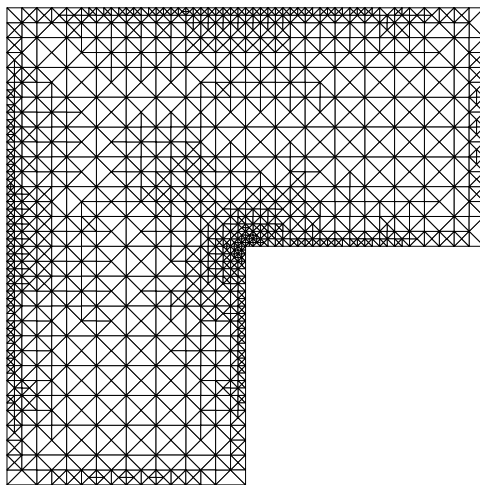


Figure 4: *The adapted mesh \mathfrak{T}_h^5 at the fifth refinement level when solving the model problem in Section 6.1.*

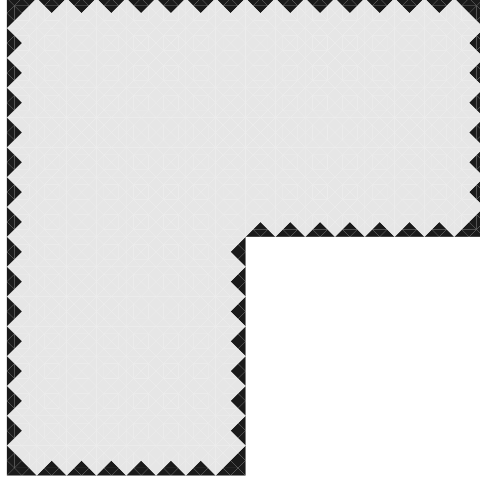


Figure 5: *The initial model distribution \mathfrak{K}_m^0 when solving the model problem in Section 6.1.*

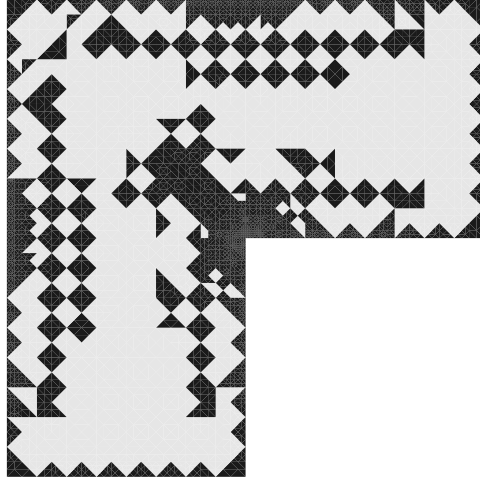


Figure 6: *The adapted model distribution \mathfrak{K}_m^5 at the fifth refinement level when solving the model problem in Section 6.1.*

Table 2: A benchmark of solving the linear systems for enhanced primal exact solutions. The execution times, with respect to systems assembled either on element patches or globally, are compared. (i is the refinement level; N_{\min} and N_{\max} are the minimum and maximum sizes, respectively, of the stiffness matrices on the element patches; t_p is the total execution time for solving all local Dirichlet problems; $\langle t_p \rangle$ is the mean execution time per element patch; N is the size of the global stiffness matrix; t_g is the execution time for solving the global system; and the speed-up, $t_g/(t_p/n)$, from solving the local Dirichlet problems in parallel assumes perfect scaling on the test system with $n = 8$ CPUs.)

i	element patches					global problem	
	N_{\min}	N_{\max}	t_p	$\langle t_p \rangle$	speed-up	N	t_g
1	181	459	2.4	$3.17 \cdot 10^{-3}$	0.36	7 553	0.1
2	181	549	2.7	$3.11 \cdot 10^{-3}$	0.42	11 445	0.1
3	181	549	3.3	$3.02 \cdot 10^{-3}$	0.72	16 977	0.3
4	181	549	4.1	$3.01 \cdot 10^{-3}$	0.73	23 921	0.4
5	211	549	5.2	$2.95 \cdot 10^{-3}$	1.02	34 241	0.7
6	211	549	6.6	$2.95 \cdot 10^{-3}$	1.16	47 573	1.0
7	211	549	8.3	$2.95 \cdot 10^{-3}$	1.34	63 201	1.4
8	211	549	10.7	$3.01 \cdot 10^{-3}$	1.39	84 981	1.9
9	211	549	13.9	$3.04 \cdot 10^{-3}$	1.81	114 341	3.1
10	181	549	17.9	$3.03 \cdot 10^{-3}$	2.63	154 913	5.9
11	181	549	23.7	$3.11 \cdot 10^{-3}$	2.32	206 765	6.9
12	211	549	29.9	$3.09 \cdot 10^{-3}$	3.79	271 877	14.1
13	211	549	39.5	$3.13 \cdot 10^{-3}$	4.47	364 617	22.1
14	211	549	52.9	$3.16 \cdot 10^{-3}$	4.66	495 793	30.8
15	211	549	71.5	$3.20 \cdot 10^{-3}$	5.70	668 781	50.9
16	211	549	93.8	$3.22 \cdot 10^{-3}$	6.25	881 965	73.4
17	211	549	126.1	$3.22 \cdot 10^{-3}$	7.47	1 192 593	117.8

Table 3: *Data during adaptive procedure when solving the model problem in Section 6.2. The error representation (17) was evaluated using enhanced discrete solutions, which were obtained by solving local Dirichlet problems. (i is the refinement level; N_{ele} is the number of elements; L is the target quantity, the maximum lateral displacement; e_{rel} is its relative error; and I_{eff} is the effectivity index.)*

i	N_{ele}	# nodes	# DOFs	$L(u^h, \theta^h)$	e_{rel}	I_{eff}
1	1 024	2 113	2 497	$8.06 \cdot 10^{-5}$	$7.12 \cdot 10^{-3}$	0.68
2	1 197	2 464	3 598	$8.06 \cdot 10^{-5}$	$7.62 \cdot 10^{-3}$	0.68
3	1 467	3 026	5 462	$8.06 \cdot 10^{-5}$	$7.32 \cdot 10^{-3}$	0.68
4	1 759	3 610	7 468	$8.07 \cdot 10^{-5}$	$6.89 \cdot 10^{-3}$	0.72
5	2 188	4 481	10 199	$8.08 \cdot 10^{-5}$	$6.23 \cdot 10^{-3}$	0.75
6	2 742	5 589	13 269	$8.10 \cdot 10^{-5}$	$5.31 \cdot 10^{-3}$	0.82
7	3 522	7 149	18 771	$8.11 \cdot 10^{-5}$	$4.60 \cdot 10^{-3}$	0.93
8	4 442	8 989	24 973	$8.12 \cdot 10^{-5}$	$3.92 \cdot 10^{-3}$	1.06
9	5 608	11 329	32 641	$8.13 \cdot 10^{-5}$	$2.68 \cdot 10^{-3}$	0.99
10	7 227	14 596	43 492	$8.13 \cdot 10^{-5}$	$2.15 \cdot 10^{-3}$	1.03
11	9 388	18 945	58 425	$8.14 \cdot 10^{-5}$	$1.70 \cdot 10^{-3}$	0.97
12	12 230	24 637	78 655	$8.14 \cdot 10^{-5}$	$1.23 \cdot 10^{-3}$	0.94

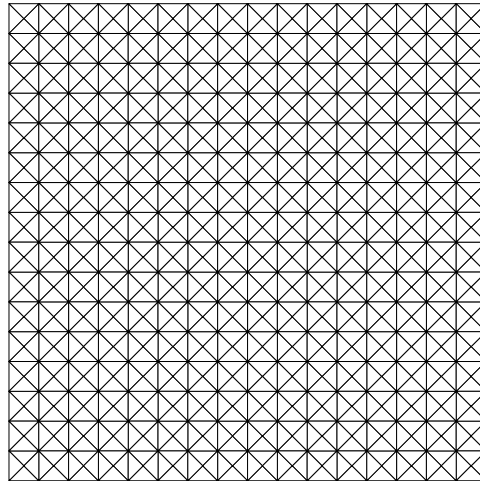


Figure 7: *The initial mesh \mathfrak{T}_h^0 when solving the model problem in Section 6.2.*

Table 4: *Data during adaptive procedure when solving the model problem in Section 6.2. The error representation (17) was evaluated using enhanced discrete solutions, which were obtained by solving global problems. (i is the refinement level; N_{ele} is the number of elements; L is the target quantity, the maximum lateral displacement; e_{rel} is its relative error; and I_{eff} is the effectivity index.)*

i	N_{ele}	# nodes	# DOFs	$L(u^h, \theta^h)$	e_{rel}	I_{eff}
1	1 024	2 113	2 497	$8.06 \cdot 10^{-5}$	$8.25 \cdot 10^{-3}$	0.78
2	1 200	2 465	3 713	$8.05 \cdot 10^{-5}$	$9.51 \cdot 10^{-3}$	0.77
3	1 504	3 097	5 641	$8.06 \cdot 10^{-5}$	$9.27 \cdot 10^{-3}$	0.81
4	1 778	3 645	7 485	$8.07 \cdot 10^{-5}$	$8.45 \cdot 10^{-3}$	0.84
5	2 124	4 337	9 905	$8.08 \cdot 10^{-5}$	$7.55 \cdot 10^{-3}$	0.91
6	2 698	5 493	13 701	$8.10 \cdot 10^{-5}$	$5.31 \cdot 10^{-3}$	0.83
7	3 496	7 089	18 309	$8.11 \cdot 10^{-5}$	$5.05 \cdot 10^{-3}$	0.99
8	4 402	8 909	24 845	$8.12 \cdot 10^{-5}$	$3.96 \cdot 10^{-3}$	1.06
9	5 478	11 061	32 295	$8.13 \cdot 10^{-5}$	$3.19 \cdot 10^{-3}$	1.13
10	7 054	14 221	42 979	$8.13 \cdot 10^{-5}$	$2.26 \cdot 10^{-3}$	1.11
11	9 200	18 553	57 673	$8.14 \cdot 10^{-5}$	$1.86 \cdot 10^{-3}$	1.12
12	12 184	24 545	77 693	$8.14 \cdot 10^{-5}$	$1.43 \cdot 10^{-3}$	1.07

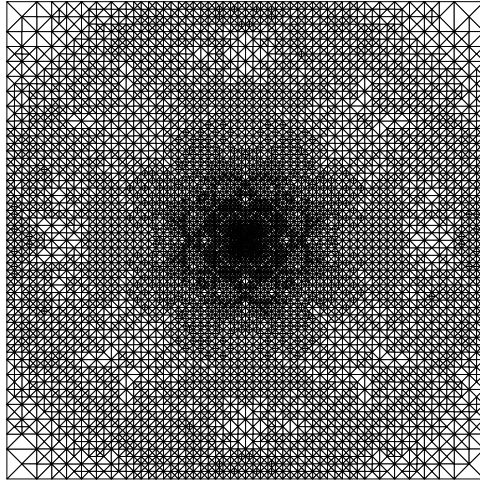


Figure 8: *The final mesh \mathfrak{T}_h^{12} when solving the model problem in Section 6.2. Constructed during adaptive procedure, where the error representation (17) was evaluated using enhanced discrete solutions, which were obtained by solving local Dirichlet problems.*

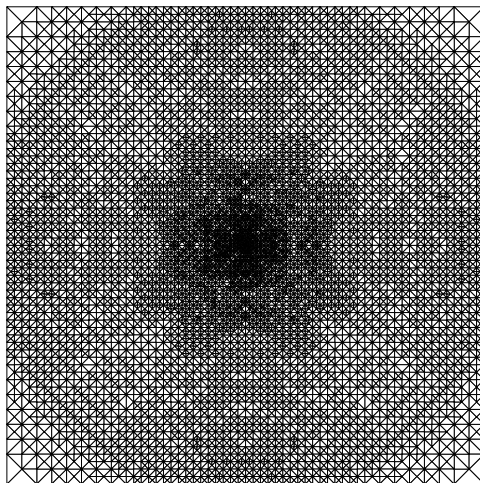


Figure 9: *The final mesh \mathfrak{T}_h^{12} when solving the model problem in Section 6.2. Constructed during adaptive procedure, where the error representation (17) was evaluated using enhanced discrete solutions, which were obtained by solving global problems.*

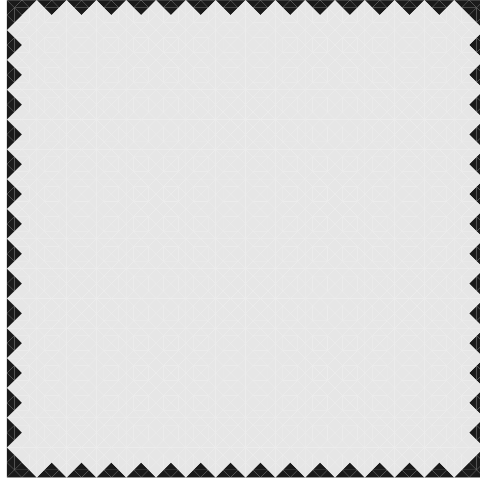


Figure 10: *The initial model distribution \mathfrak{R}_m^0 when solving the model problem in Section 6.2.*

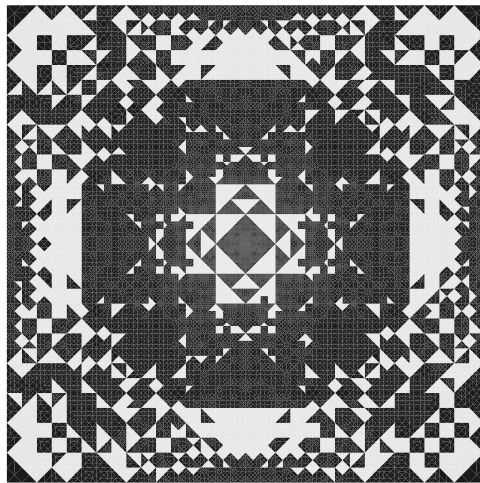


Figure 11: *The final model distribution \mathfrak{R}_m^{12} when solving the model problem in Section 6.2. Constructed during adaptive procedure, where the error representation (17) was evaluated using enhanced discrete solutions, which were obtained by solving local Dirichlet problems.*

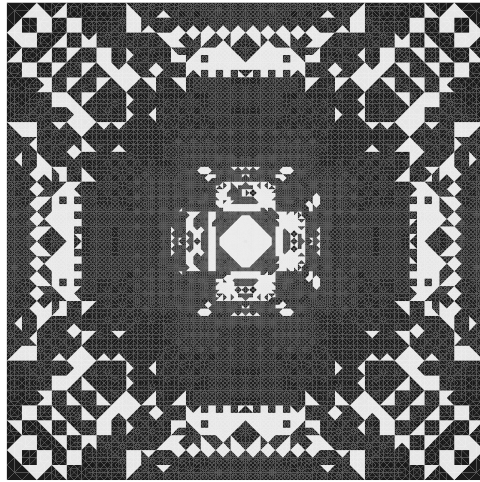


Figure 12: *Final model distribution \mathfrak{R}_m^{12} when solving the model problem in Section 6.2. Constructed during adaptive procedure, where the error representation (17) was evaluated using enhanced discrete solutions, which were obtained by solving global problems.*